ACS APPLIED MATERIALS & INTERFACES

www.acsami.org

Research Article

Tunable Pore Size from Sub-Nanometer to a Few Nanometers in Large-Area Graphene Nanoporous Atomically Thin Membranes

Xiaobo Chen, Shengping Zhang, Dandan Hou, Hongwei Duan, Bing Deng, Zhiyang Zeng, Bingyao Liu, Luzhao Sun, Ruiyang Song, Jinlong Du, Peng Gao, Hailin Peng, Zhongfan Liu, and Luda Wang*

Cite This: *ACS Appl. Mater. Interfaces* 2021, 13, 29926–29935

Read Online

ACCESS | Metrics & More | Article Recommendations | Supporting Information

ABSTRACT: Membranes are key components in chemical purification, biological separation, and water desalination. Traditional polymeric membranes are subjected to a ubiquitous trade-off between permeance and selectivity, which significantly hinders the separation performance. Nanoporous atomically thin membranes (NATMs), such as graphene NATMs, have the potential to break this trade-off. Owing to their uniqueness of two-dimensional structure and potential nanopore structure controllability, NATMs are expected to have outstanding selectivity through molecular sieving while achieving ultimate permeance at the same time. However, a drastic selectivity discrepancy exists between the proof-of-concept demonstrations and scalable separation applications in graphene membranes. In this paper, we offer a possible solution to narrow this discrepancy by tuning the pore density and pore size separately with two successive plasma treatments. We demonstrate that by narrowing the pore size distribution, the selectivity of graphene membranes can be greatly increased. Low-energy argon plasma is first applied to nucleate high density of defects in graphene. Controlled oxygen plasma is then utilized to selectively enlarge the defects into nanopores with desired sizes. This method is scalable, and the fabricated 1 cm^2 graphene NATMs with sub-nanometer pores can separate KCl and Allura Red with a selectivity of 104 and a permeance of 1.1×10^{-6} m s^{-1}. The pores in NATMs can be further tuned from gas-selective sub-nanometer pores to a few nanometer size. The fabricated NATMs show a selectivity of 35 between CO_2 and N_2. With longer enlargement time, a selectivity of 21.2 between a lysozyme and bovine serum albumin can also be achieved with roughly four times higher permeance than that of a commercial dialysis membrane. This research offers a solution to realize NATMs of tunable pore size with a narrow pore size distribution for different separation processes from sub-nanometer in gas separation or desalination to a few nanometers in dialysis.

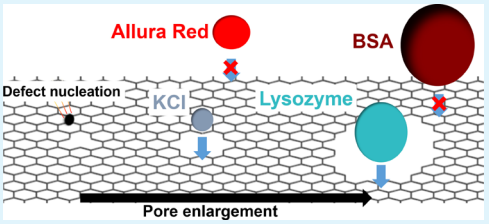

KEYWORDS: *nanoporous graphene membranes, nanoporous atomically thin membranes (NATMs), protein-selective membranes, plasma etching, nanopore engineering*

1. INTRODUCTION

Membrane separation is an energy-efficient method for separating chemical species[1] and has been widely adopted in industry due to its simplicity and high energy efficiency.[1−3] The fast development of separation industry demands for more advanced membranes that have both superior selectivity and permeance.[4] Traditional polymeric membranes usually use a dense layer to function as a selective molecular barrier. Permeance of certain molecules is mainly controlled by their solubility and diffusivity in this barrier material according to solution-diffusion mechanisms.[5] Also, the selectivity between certain species is a result of different solubilities and diffusivities. For many polymeric membranes, the selectivity is mainly influenced by the sizes or size distribution of these free-volume elements.[6] However, increasing the free-volume element size to achieve higher permeation usually results in lower selectivity. This is because the permeability enhancement of larger species is more significant than that of smaller species due to the inability to control the polymer chain structure in sub-nanometer precision.[6,7] Thus, polymeric membranes are subjected to a ubiquitous trade-off between permeability and selectivity.[7−10] In this regard, new materials with the ability of molecular sieving, such as zeolites, metal−organic frameworks, two-dimensional (2D) materials, and other novel materials, have been used in membrane separation due to their highly controlled nanopores structures.

Among these materials, graphene nanoporous atomically thin membranes (NATMs) are expected to be a promising candidate for membrane technology.[11−14] Owing to their uniqueness of two-dimensional structure, graphene NATMs with high nanopore density are expected to have outstanding selectivity through molecular sieving while maintaining their ultimate permeance. In addition, excellent mechanical and

Received: April 5, 2021
Accepted: May 27, 2021
Published: June 16, 2021

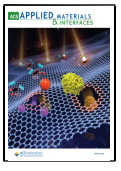

https://doi.org/10.1021/acsami.1c06243
ACS Appl. Mater. Interfaces 2021, 13, 29926−29935

chemical stability makes graphene more tolerant to harsh operation conditions than polymeric membranes.[2] Moreover, compared to other 2D materials, the fabrication of high-quality large-area graphene is scalable.[15] The selectivity of NATMs largely depends on the quality of nanopores in them. Some pioneer works have demonstrated that graphene with a limited number of nanopores could achieve molecular-sieving selectivity or complex switching behavior.[16−18] Also, calculation showed that with well-controlled nanopores, the graphene NATMs could easily exceed the polymeric upper bond with a pore density of 10^{10} cm^{-2}.[19] However, the experimental work showed that the selectivity of NATMs could be drastically decreased to a number close to the Knudsen selectivity with a comparable pore density (5.4×10^{10}).[20] This decrease in selectivity at higher density can be viewed as the inability to control the pore size distribution during nanopore generation. The calculation works often assume that the NATMs have high-density nanopores with a narrow pore size distribution,[19] whereas this is hard to be achieved in scalable methods. Generally, nanopore generation in graphene starts with defect nucleation and is further enlarged into nanopores with desirable sizes. Simultaneously introducing pore creation and enlargement in conventional etching methods often leads to a trade-off between pore density and the pore size distribution. The defects or grain boundaries of graphene often have a much higher reactivity than the perfect graphene lattice[21] and are thus more vulnerable during etching. Thus, increasing the defect density often results in the formation of larger pores at those areas and broadening of the pore size distribution. As a result, it is hard for the scalable one-step method to fabricate NATMs with both high density and a narrow pore size distribution due to the uncontrolled etching reaction. Bottom-up methods can fabricate graphene-like materials with highly ordered pore structures or introduce nanopores by changing the growth environments.[22,23] However, accurately controlling the pore structure by bottom-up methods is still challenging due to the synthetic difficulty.[24,25] Top-down methods can introduce nanopores on previously fabricated graphene with a wider pore size distribution. Oxygen plasma was used to introduce nanopores into graphene, and a water flux of 10^6 g m^{-2} s^{-1} was achieved.[26] However, increasing the permeance solely by oxygen plasma resulted in the decrease in selectivity, suggesting a similar permeance selectivity trade-off.[26] To overcome this trade-off, different methods have been applied to either narrow the nanopore size distribution or increase nanopore density.[27−31] However, these methods often involved hazardous chemicals like hydrofluoric acid or required a complicated FIB system and were time-consuming even for laboratory demonstrations (~10 cm^2).[7] For example, it would take up to tens of minutes for the FIB system to process a centimeter-large area, as it needs several microseconds to bombard ions onto each pixel.[30] Moreover, the pore size distribution was often broadened during the following etching, hindering the performance of NATMs.[29,30,32]

In this paper, we demonstrated that by decoupling pore creation and pore enlargement during nanopore generation, the selectivity of graphene NATMs could be greatly increased with little influence on its permeance, thus narrowing the selectivity discrepancy between the proof-of-concept demonstrations and scalable separation applications. Furthermore, the pore density and pore size can be tuned with two successive plasma treatments. Low-energy argon plasma and cage-protected oxygen plasma were applied to control the pore density and pore size, respectively. Argon plasma can introduce defects into graphene lattices as the pore creation sites through ion bombardment effects. The density of the nanopores can be tuned by adjusting the number of ions that are bombarded onto graphene. Oxygen plasma was then utilized to selectively enlarge the previously introduced defects into nanopores, and the pore size could be controlled by the oxygen plasma conditions. NATMs fabricated by the decoupling method showed greatly enhanced performance compared to the NATMs fabricated by traditional methods. With optimized conditions, a selectivity of 104 between KCl and Allura Red was achieved with a KCl permeance of 1.1×10^{-6} m s^{-1} in diffusion-driving separation tests. By varying the pore enlargement time, the sizes of nanopores could be tuned from gas-selective sub-nanometer to a few nanometers that are protein-selective. The fabricated NATM with only 10 s oxygen plasma treatment showed a selectivity of 39 between CO_2 and N_2. Increasing the oxygen treatment time could further enlarge the nanopores to separate a lysozyme and bovine serum albumin, two solutes that have comparable sizes to β2-microglobulin and human serum albumin, with a selectivity of 21.2 and roughly four times higher permeance than the commercial dialysis membrane. The decoupling of pore creation and pore enlargement shown in this paper could be a key standard of introducing nanopores with high density and a narrow pore size distribution to 2D materials and provide a universal method for fabricating the NATMs for different separation processes from sub-nanometer in gas separation, desalination, or ion separation to a few nanometers in nanofiltration or dialysis.

2. EXPERIMENTAL SECTION

2.1. Graphene Growth. Graphene was fabricated using a low-pressure chemical vapor deposition (LPCVD) method. Copper foil was purchased from Sichuan Oriental Stars Trading Co., Ltd. To clean the surface of copper foil, electropolishing was performed using a mixture of phosphoric acid and glycol with a volume ratio of 3:1 at 1.5 V for 15 min. After that, copper foil was further cleaned using deionized (DI) water and ethanol subsequently. The Cu foil was dried in nitrogen. The cleaned copper foil was directly put into a CVD chamber and annealed for 60 min at 1025 °C in a 400 sccm H_2 atmosphere. Then, 4 sccm of methane was introduced into the chamber to allow graphene growth. The growth time was set to 2 h to get full coverage of graphene. Then, copper foil was quickly cooled to room temperature in the same atmosphere. After growth, the graphene sample was stored in a vacuum chamber.

2.2. Graphene Transfer. Graphene was transferred to a polycarbonate track-etched (PCTE) membrane through a modified hot-press method. Before transfer, 10 min sodium persulfate etching was applied to remove the back side of graphene on copper. Subsequently, graphene and the PCTE were gently pressed together under 100 °C for 10 h. After pressing, another sodium persulfate etching was performed to fully etch the copper away, leaving graphene on the PCTE. The PCTE-graphene composite was cleaned with deionized water followed by ethanol rinsing and dried at room temperature. The composite was further annealed in an oven at 110 °C for 10 h to get better contact.

2.3. Interfacial Polymerization. To minimize the influence of unselective cracks on the graphene membrane, interfacial polymerization was adopted on the graphene-PCTE. The detailed method can be found in other papers.[23] In short, 2 g/L piperazine and 0.2 g/L trimesoyl chloride were introduced to the two sides of the PCTE. Piperazine and trimesoyl chloride would quickly form a dense polymer plug in the holes in the PCTE if graphene was broken during

https://doi.org/10.1021/acsami.1c06243
ACS Appl. Mater. Interfaces 2021, 13, 29926−29935

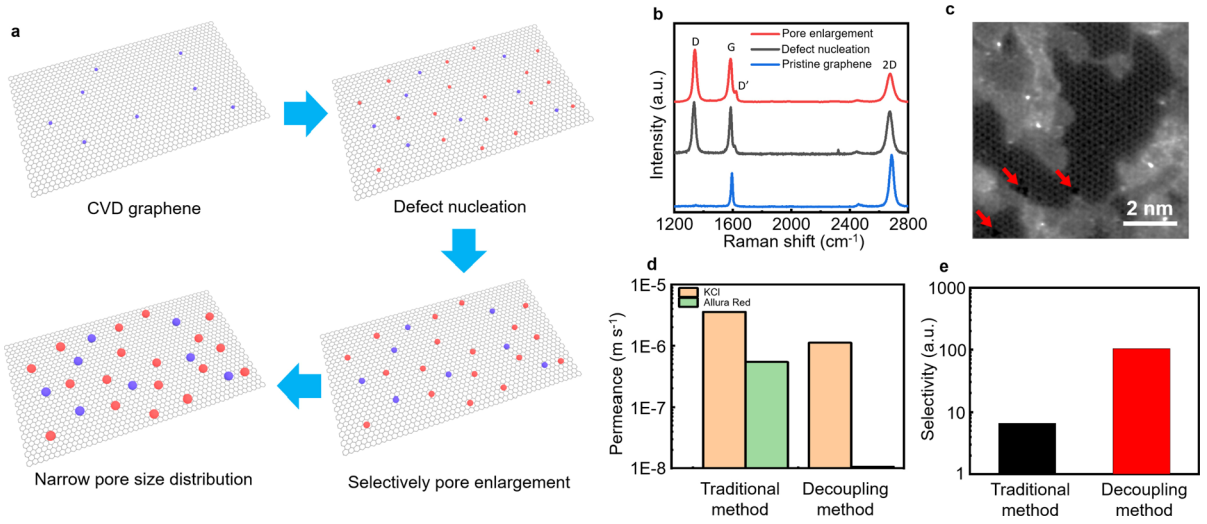

Figure 1. Illustration of the decoupling method, characterization of graphene NATMs, and performance comparison of graphene NATMs prepared by the traditional method and the decoupling method. (a) Illustration of the decoupling method leading to a narrow pore size distribution. (b) Comparison of Raman spectra of pristine graphene, defect-nucleated graphene, and pore-enlarged graphene. (c) Atomically resolved image of treated graphene. The nanopores are marked using red arrows for better illustration. (d) Permeance of KCl and Allura Red of NATMs prepared using the traditional method and the decoupling method. (e) Calculated selectivity of KCl to Allura Red based on the permeance data in (d).

transfer. As a result, cracks and tears were sealed and would not influence the following tests.

2.4. Plasma Etching. A two-step plasma treatment was adopted to generate desired pores on graphene. First, argon plasma was applied to graphene to nucleate defect sites in it. The power of argon plasma was set to 20 W, and pressure was ~160 Pa. Then, oxygen plasma was introduced to enlarge the pores with the protection of a Faraday cage. The power of oxygen plasma was 7 W. Direct plasma treatment was found to be too strong for argon-treated graphene, so a Faraday cage was applied to give a mild etching environment in the oxygen plasma treatment. The Faraday cage was made of a steel cylinder with a porous steel net at the top. The pore size of the net was about 6.5 μm.

2.5. Characterization. SEM images were recorded using a Hitachi S-4800. Raman spectra were obtained using a Horiba LabRAM HR800 with a 532 nm laser. All the Raman data were obtained after transferring the corresponding graphene onto a silicon wafer with a SiO_2 layer. Standard TEM images were obtained using an FEI Tecnai F20. High-angle annular dark-field (HAADF) images were recorded on a Nion U-HERMES200 aberration-corrected STEM operated at an accelerating voltage of 60 kV. Before the STEM experiments, the samples were annealed at 160 °C for 8 h to remove any hydroxide contamination. The convergence semi-angle was 35 mrad with an annular recording range of 80−210 mrad. The electron probe diameter was focused to ~60 pm. The beam current was measured to be 28 pA for the STEM imaging. The STEM images were recorded with 2048 × 2048 pixels, and each pixel collection time was 128 ms.

2.6. Diffusion Tests. To perform diffusion tests, graphene NATMs were placed between two side-by-side cells, and the cells were firmly pressed together using a holder to prevent leakage. Both sides were first rinsed with ethanol to wet the PCTE membrane and rinsed with DI water 3 min for three times prior to tests. For diffusion-driven tests, potassium chloride (0.33 nm, hydrated radius of K^+), sodium chloride (0.36 nm, hydrated radius of Na^+), Allura Red (~0.5 nm, Stokes−Einstein molecular radius), a lysozyme (MW of ~14,000), and bovine serum albumin (MW of ~66,000) were selected to evaluate the performance of the sample. A solution with a certain concentration of a model solute was placed to the feed side of the flow cell, and the same volume of DI water was placed to the permeate side. Slowly, the solute would diffuse across the membrane into the permeate side driven by the concentration difference of the solute between the two sides. The increasing concentration of the solute in the permeate side was recorded for further analysis. For potassium chloride and sodium chloride, the concentration of the feed solution was 0.5 mol/L, a conductive probe was used to detect the concentration in the permeate side, and the increase rate was calculated using 5 min data. For Allura Red, the concentration was 10^{-3} mol/L. Also, a UV−vis spectrometer was used to measure the concentration in the permeate side. The difference in UV−vis spectra of the reference point at 710 cm^{-1} and the Allura Red peak at 510 cm^{-1} was used to compute the concentration of Allura Red, and the increase rate was calculated using at least 15 min data. For the lysozyme, the concentration was 5 g/L, the difference of 710 and 282 cm^{-1} was used to compute the concentration, and the increase rate was calculated using at least 30 min data. For BSA, the concentration was 5 g/L, the difference of 710 and 280 cm^{-1} was used to compute the concentration, and the increase rate was calculated using at least 30 min data. To minimize the concentration polarization, two sides were stirred at 600 rpm.

2.7. Gas Leak Rate Measurement. To fabricate the microcavity, mechanically foliated graphene was first transferred onto the silicon well with a radius of 1.5 μm and a depth of 1 μm. To introduce gas-selective nanopores, graphene was treated with 10 s of argon plasma and 10 s of oxygen plasma as the pore nucleation and pore enlargement steps, respectively. Before AFM measurement, the microcavities were first put into a pressurized chamber of 2 × 10^5 Pa for about 1 or 2 days to inflate them. After pressurization, the microcavities were taken out from the chamber, and the deflections of microcavities were measured using a Bruker Dimension Icon using tapping mode at atmospheric pressure. The gas molecules would transport through the preintroduced sub-nanometer pores, causing the deflection decrease in graphene NATMs. Thus, the deflection drop rate can be used to evaluate the gas leak rate of NATMs.

3. RESULTS AND DISCUSSION

3.1. Synthesis, Characterization, and Performance of Graphene NATMs by the Decoupling Method. To separate pore creation and pore enlargement, a specifically designed pore engineering method was applied to introduce nanopores into graphene with two plasma treatment steps. The defects were first introduced into graphene by argon plasma treatment. Then, pore enlargement was performed using controlled oxygen plasma to selectively enlarge the defects (Figure 1a). Since all the defects shared the same pore

https://doi.org/10.1021/acsami.1c06243
ACS Appl. Mater. Interfaces 2021, 13, 29926−29935

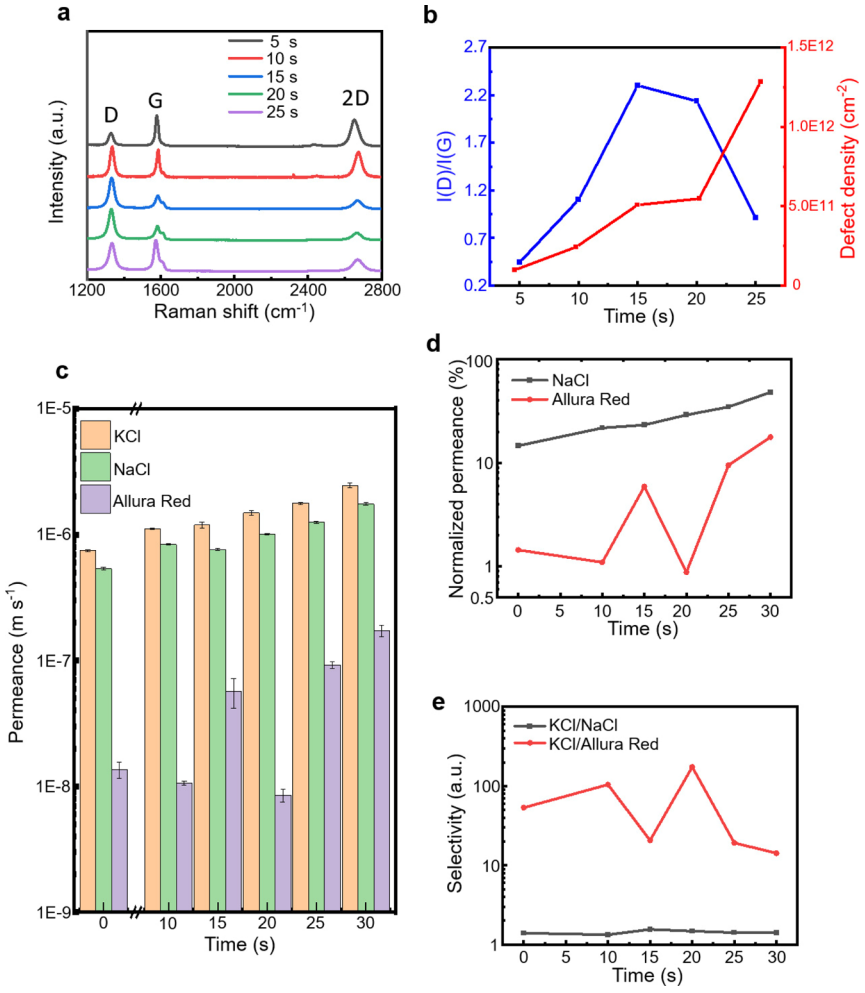

Figure 2. Influence of argon plasma time on graphene NATMs. (a) Influence of argon plasma on Raman spectra. (b) Derived $I(D)/I(G)$ and defect density calculated from $I(D)/I(G)$. (c) Influence of argon plasma time on the permeance of different solutes. (d) Normalized permeance of KCl and Allura Red. (e) Corresponding selectivity of KCl to NaCl and KCl to Allura Red.

enlargement time, a narrow pore size distribution was achieved. This method is based on the observation that enlargement of nanopores is easier than pore creation in the intact graphene lattice, as the defects have much higher chemical reactivity than the intact graphene lattice. Calculation showed that in oxygen plasma conditions, the oxygen atoms could form an epoxy structure on the perfect graphene lattice, and the energy barrier of the following desorption of CO was about 4.8 eV, whereas at the defects, the oxygen atoms would form a lactone-like structure, which eventually led to the desorption of carbon oxides with a reduced barrier less than 2 eV.[33] In this case, it is possible to introduce defects into graphene through ion bombardment and selectively enlarge the defects with a controlled chemical etching environment.

The graphene used in ion or protein separations was synthesized by LPCVD on copper with longer time to ensure full coverage of graphene and to facilitate the growth of few-layer graphene islands.[15] Raman spectra were used to evaluate the quality of graphene.[34−36] The Raman spectrum of pristine graphene showed two identical graphene peaks: a G peak at 1580 cm^{-1} and a 2D peak at 2680 cm^{-1} (Figure 1b). No obvious defect peak at 1350 cm^{-1} was found, evidencing the minimum intrinsic defects of pristine graphene. Also, the ratio of $I(G)$ to $I(2D)$ was about 0.6. This value was close to the characteristic value of single-layer graphene[37,38] and smaller than that of double-layer graphene.[39] Previous works have shown that the intensity of the G peak increased monotonically until reaching ten or more layers, while the intensity of the 2D peak decreased with the increase in layer numbers.[34,40,41] We thus concluded that our graphene was mainly one layer with few-layer islands. These few-layer islands usually share the same nucleate centers of the first layer, which contain highly reactive defects.[42] Thus, additional layers could serve as natural patches to defective areas, minimizing the formation of larger pores or tears in the following treatment. The creation of defects by argon plasma is through the ion bombardment effect that the energetic argon ions knock off the carbon atoms, creating single vacancy defects in graphene.[43,44] Controlling the number of ions that are bombarded onto graphene can thus control the defect density of graphene. Moreover, recent research suggested that the defects at grain boundaries could even be healed during low-energy argon plasma treatment through preferential migration of carbon adatoms on the graphene surface.[45] In this regard, we applied argon plasma at moderate pressure (~200 Pa) with low power (~20 W) to control the defect density in graphene. After argon plasma, the D peak was clearly observed in the Raman spectrum (Figure 1b). Besides the D peak, the D′ peak (~1620 cm^{-1}) was also observed. The enlargement of preintroduced defects was achieved using controlled oxygen plasma treatment. The

https://doi.org/10.1021/acsami.1c06243
ACS Appl. Mater. Interfaces 2021, 13, 29926−29935

energetic oxygen ions or atoms in oxygen plasma can chemically etch graphene, creating vacancy-type defects or nanopores with the release of CO or CO_2.[46] A custom-designed Faraday cage was applied to reduce the energy of oxygen ions or oxygen atoms of oxygen plasma, thus minimizing the etching effect at the perfect graphene lattice. The Raman spectra showed a similar ratio of $I(D)/I(G)$ before and after 1 min oxygen plasma treatment, proving that the oxygen plasma treatment did not obviously increase defect density. However, the $I(D)/I(D')$ ratio dramatically decreased, indicating a transformation of previously introduced predominantly Stone−Wales (an in-plane 90° rotation of the C−C bond with respect to the midpoint of the bond) or sp^3-type defects (carbon hybridization from sp^2 to sp^3) into vacancy-like nanopores as reported by other works.[36,47−49] Aberration-corrected scanning transmission electron microscopy (AC-STEM) was applied to further study the nanopore structure of graphene NATMs (Figure 1c). The graphene sample had the same treatment condition as the pore-enlarged sample used in Figure 1b. Three nanopores were found with an area of 64 nm^2. The pore density was estimated to be about 5.7×10^{11} cm^{-2} using a total of 30 atomically resolved images. More atomically resolved images and TEM images for pristine graphene and defect-nucleated graphene could be found in Supplementary Section 3. Diffusion-driven separation tests were applied to investigate the improvement on performance of graphene NATMs.[50] Graphene was first transferred onto a porous polycarbonate track-etched (PCTE) membrane. The PCTE membrane has well-controlled physical properties and similar separation performance between different chips. The concentration gradient drove the solutes to the permeate side through the NATMs. By measuring the concentration changes, the performance of the membrane was obtained. The SEM images of graphene on the PCTE substrate showed good coverage with few tears (Figure S6). These tears were further sealed by interfacial polymerization (IP) to minimize their influence on the result. We compared the performance of NATMs fabricated by the decoupling method and the traditional method to demonstrate the advantage of the decoupling method. KCl and Allura Red were chosen as model solutes for separation experiments. For better comparison, the treatment time of oxygen plasma was increased to 2 min. The NATMs fabricated using the conventional plasma etching method[30] were chosen as the control group. Figure 1d shows the permeance of graphene NATMs fabricated by the conventional method and the decoupling method. Figure 1e shows the corresponding selectivity data of NATMs prepared by those two different methods. As can be seen, the decoupling method greatly increased the selectivity with no substantial decrease in permeance.

3.2. Controlling Nanopore Density by Argon Plasma. As discussed before, argon plasma can effectively tune pore density in graphene NATMs by changing the number of bombarded argon ions. Raman spectra showed that longer argon treatment could increase the defect density in graphene by providing more argon ions bombarded onto graphene. The D peak quickly increased, and the G peak and the 2D peak decreased with longer argon plasma time (Figure 2a). According to previous papers, the ratio of $I(D)/I(G)$ can be used as an evaluation of defect density.[35,47,48,51,52] At the low defect density regime, the $I(D)/I(G)$ increased with increasing defect density, whereas at the high defect density regime, $I(D)/I(G)$ decreased.[35] With the increase in plasma treatment time, $I(D)/I(G)$ rapidly increased to 2.3 at 15 s (Figure 2b). After 15 s, $I(D)/I(G)$ started to decrease, corresponding to a transition from the low defect density regime to the high defect density regime. The calculated defect density of different treatment times was also summarized (Figure 2b). Argon treatment could effectively increase defect density up to around 1.3×10^{12} cm^{-2} on graphene at 25 s (the detailed calculation method can be seen in Supplementary Section 2). Furthermore, the D′ peak also emerged after 15 s argon plasma treatment. To minimize the overlapping of neighboring nanopores, the optimum argon plasma treatment time was set to be 10 s in this study. The argon plasma-treated samples were further treated with 2 min oxygen plasma treatment to enlarge the defects into nanopores. KCl, NaCl, and Allura Red were chosen as model solutes to evaluate the performance of the NATMs. The permeance was summarized to compare the influence of argon treatment time (Figure 2c). As the defect density at 5 s was relatively small, we measured the permeance of NATMs with at least 10 s argon treatment. It can be observed that with a longer treatment time, the permeance of all the solutes increased. Ideally, if pore size solely depended on oxygen plasma, then increasing defect density should only increase the permeance and maintain the selectivity. However, higher density of nanopores would inevitably result in a higher possibility of merging of nearby nanopores. After 25 s, the defect distance was around 5 nm, suggesting that this tendency might be very common at the high-density region of nanopores (the calculation of defect distance could be found in Supplementary Section 2). To compare the permeance evaluation of KCl and Allura Red, the data were normalized by the corresponding permeance of the PCTE. The normalized fluxes of KCl and Allura Red clearly showed this tendency (Figure 2d). The flux of KCl and Allura Red both increased with plasma time similar to the increase in defect density. Yet, the flux of Allura Red experienced more fluctuations than that of KCl. This can be explained by that after oxygen plasma treatment, the nanopores were already large enough to allow the transport of KCl, yet most of the nanopores still forbade the transport of Allura Red. In diffusion-driven tests, the permeance of certain solutes is in linear relationship to the open area.[53] Thus, the merging of nearby nanopores had less influence to KCl than Allura Red because the open area for KCl to transport was almost unchanged when the nearby pores merged into one bigger pore, whereas a larger pore would permit the transport of Allura Red (a more detailed discussion of merging can be found in Supplementary Section 5). This also caused the selectivity between KCl and Allura Red to first increase and then decrease (Figure 2e). The selectivity of two small solutes, like KCl and NaCl, was almost unchanged because the nanopores were already too large to distinguish these two solutes.

3.3. Controlled Oxygen Plasma Selectively Enlarges the Defects. The nanopore size could be tuned by oxygen plasma conditions. A Faraday cage was applied to achieve selective enlargement at the previously introduced defects. The Faraday cage can effectively screen the electric field and has been used in PECVD graphene growth.[54] With the Faraday cage, oxygen plasma would tend to mainly enlarge sp^3-type or Stone−Wales-type defects into nanopores, as the energy of oxygen species inside the cage was greatly reduced. The Raman spectra revealed that with 1 min oxygen plasma treatment, the $I(D)/I(G)$ was almost unchanged (Figure 3a) from the defect-nucleated sample, indicating that the defect density should be

https://doi.org/10.1021/acsami.1c06243
ACS Appl. Mater. Interfaces 2021, 13, 29926−29935

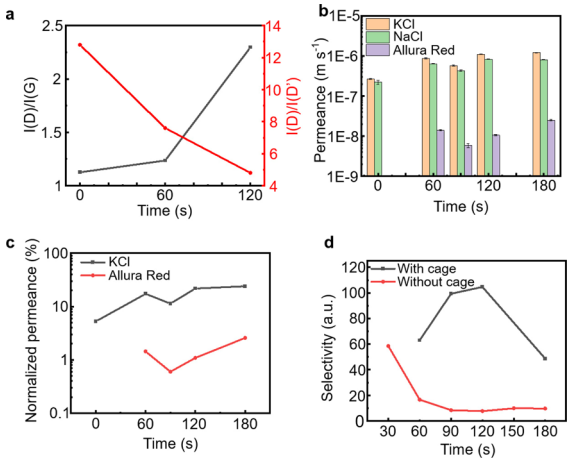

Figure 3. Influence of oxygen plasma on graphene NATMs. (a) Influence of oxygen plasma on the $I(D)/I(G)$ and $I(D)/I(D')$. (b) Influence of oxygen plasma time on permeance of different solutes. (c) Normalized permeance of KCl and Allura Red under different oxygen plasma times. (d) The Faraday cage greatly improved the selectivity of KCl to Allura Red under different oxygen plasma times.

similar after 1 min oxygen plasma treatment. However, with the further treatment, a notable increase in $I(D)/I(G)$ could be observed. We attribute this increase to the increase in pore size as a previous paper reported that a larger defect size would have a higher $I(D)/I(G)$.[55,56] A detailed discussion can be found in Supplementary Section 7. On the contrary, the $I(D)$ to $I(D')$ ratio quickly dropped. The vacancy-like defects usually have a lower $I(D)/I(D')$ ratio than the Stone−Wales or sp^3-type defects, and thus, the $I(D)/I(D')$ ratio can be used to distinguish the defect type of graphene.[36,47−49] A previous report showed that the sp^3-type defects usually had a ratio of about 13 while the ratio of vacancy-type defects dropped to about 7.[48] After 1 min oxygen plasma treatment, the $I(D)/I(D')$ ratio quickly decreased from ∼13 to ∼8 (Figure 3a), indicating the enlargement of previously introduced defects into vacancy-like nanopores. The permeance of corresponding graphene NATMs is shown in Figure 3b. To compare the permeance evaluation of these two solutes, the data were normalized by the corresponding permeance of the PCTE (Figure 3c). The permeance of KCl increased much slower than that of Allura Red. With longer oxygen plasma treatment time, the size of nanopores increased and permitted the transport of Allura Red, thus resulting in a faster permeance increase. Simulation results showed that the Faraday cage offered a much milder plasma environment.[57] The plasma was screened by the Faraday cage, and the electric field inside it was greatly reduced (simulation details can be seen in Supplementary Section 4). As a result, oxygen ions or atoms arrived at graphene with lower kinetic energy. Thus, cage-protected oxygen plasma might selectively etch the defect sites. The results showed that the cage-protected samples had a higher selectivity over unprotected ones, as expected (Figure 3d).

3.4. The Separation of Gas Molecules and Few-Nanometer-Sized Proteins by Graphene NATMs. With the decoupling method, precisely controlling the size of nanopores in NATMs over a wide range with no obvious broadening of the pore size distribution might be possible. We demonstrated the gas molecular sieving ability of the fabricated sample by measuring the change in deflection from a pressurized microcavity covered by NATMs.[16] To achieve gas-selective sub-nanometer pores, we enlarged the defects with only 10 s oxygen plasma treatment after defect nucleation. Figure 4a showed the calculated leak rate of three different gases, with the diameter ranging from 0.33 nm of CO_2 to 0.36 nm of N_2. The selectivity of CO_2 and N_2 was about 39, which was much higher than the Knudsen selectivity (∼1.3), evidencing the introduction of molecular sieving sub-nanometer pores. This method could also fabricate NATMs with nanopores of a few nanometers by changing the treatment conditions. The conventional polymeric dialysis membranes usually have a wide pore size distribution and are thus unable to separate proteins within a 10-fold difference in molecular weight.[58] In hemodialysis, one of the bottlenecks is the removal of large-size toxins (i.e., β-microglobulin, MW of ∼11,800) while retaining the normal blood composite (i.e., human serum albumin, MW of ∼67,000). The lysozyme (MW of ∼14,000) and BSA (MW of ∼66,000) were intentionally chosen as the marker solutes due to their similar sizes. The commercial dialysis membrane showed almost no selectivity (∼1) of BSA to the lysozyme and low permeance. In contrast to a traditional polymer membrane, the NATMs showed much higher selectivity (21.2) between the lysozyme and BSA and around four times higher permeance than the commercial membrane (Figure 4b). The result confirmed that with a well-controlled pore size distribution, the graphene NATMs can outperform the commercialized polymeric membranes in both

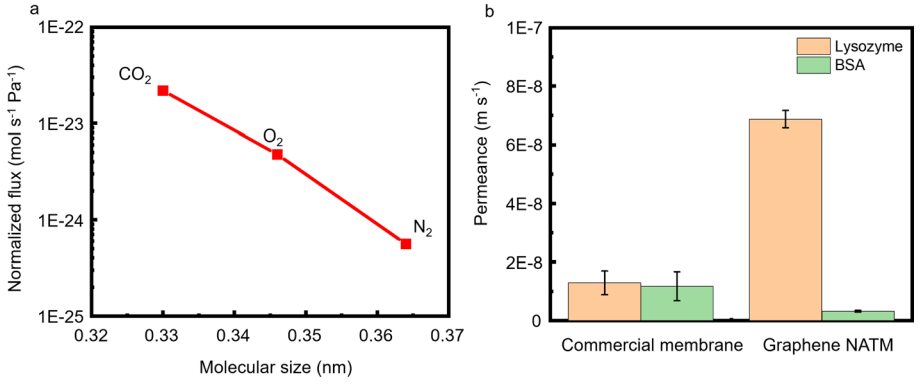

Figure 4. Tunable pore size of the decoupling method from gas-selective sub-nanometer pores to protein-selective nanopores. (a) Normalized gas leak rate of graphene NATMs with shorter oxygen plasma treatment time. (b) Permeance comparison between graphene NATMs and a commercial dialysis membrane.

https://doi.org/10.1021/acsami.1c06243
ACS Appl. Mater. Interfaces 2021, 13, 29926−29935

permeance and selectivity. Moreover, the selectivity of graphene NATMs was notably higher than the selectivity achieved by isoporous membranes,[59−61] molecularly imprinted cryogel membranes,[62] silica colloidal crystal membranes,[63] and track-etched membranes.[64] Also, this value was comparable to the selectivity achieved in diffusion tests by gold nanotubule membranes.[65] The graphene NATMs with superior permeance might be a promising candidate for portable hemodialysis, which requires the dialysis membrane to have better permeance and selectivity to remove kidney toxins, thus achieving efficient water utilization or miniaturization.[66]

3.5. Further Discussions. Overcoming the trade-off between permeability and selectivity is one of the vital challenges in membrane technology. To solve this problem, novel materials and mechanisms are required to be applied to membranes and clarify the transport processes. Graphene NATMs, with the ability of molecular sieving, are predicted to have both outstanding selectivity and permeance.[7] The selectivity of NATMs mainly depends on the pore size distribution in them. Though NATMs with a limited number of nanopores showed a molecular sieving ability, the selectivity drastically decreased at higher density (i.e., 10^{10} cm^{-2}) due to a wide pore size distribution. We successfully introduced a single nucleation event by plasma etching and achieved a narrow pore size distribution, as inspired by the synthesis of monodisperse nanocrystals (nucleation and growth).[67−69] This single nucleation event can (1) guarantee the same enlargement time for all the nanopores and (2) minimize the overlapping of neighboring pores by preventing the formation of unwanted smaller pores. Minimization is especially important in introducing larger pores at higher density. Moreover, pore density and pore size can be solely controlled by different plasma treatment steps. Low-energy argon plasma was used to introduce sp^3-type or Stone−Wales defects into graphene as pore creation sites by ion bombardment effects, and the pore density can be controlled by changing the treatment time. With the protection of a Faraday cage during oxygen plasma treatment, oxygen plasma tended to mainly enlarge the size of previously introduced defects, and the unwanted defect nucleation was suppressed. Varying the oxygen plasma treatment time can thus be used to tune the pore size of NATMs. Also, this tunability of pore size is urgently needed to improve the performance of certain separation processes.[7] For instance, increasing the selectivity of RO films is highly valued in desalination for improving the quality of product water.[8] On the other hand, the only-water-permeate smaller pores have little contribution to the removal of larger uremic toxins, and the increase in pore size to remove larger peptide and protein toxins is urgently needed in hemodialysis membranes.[70,71]

4. CONCLUSIONS

In conclusion, we demonstrated that the pore density and pore size of graphene NATMs can be thoroughly decoupled and separately controlled with two plasma steps. Diffusion tests showed that the selectivity of KCl to Allura Red was greatly increased with no substantial decrease in permeation compared to nanopores introduced by the traditional pore creation method. Moreover, this method could effectively tune the pore size from sub-nanometer to a few nanometers. Experimental results proved that our NATMs not only had a gas separation ability but also had much higher selectivity between two proteins as well as higher permeance than commercial dialysis membranes. Our method provided an effective solution to tune not only the defect density but also the pore size of graphene NATMs, which might be a universal method for different separation applications from gas separation, desalination, or ion separation to nanofiltration. In addition, this method might also be applied to other 2D materials. Also, for graphene itself, the graphene NATMs, which have superior selectivity and permeability over polymeric membranes, might be one of the striking applications that the graphene industry calls for.

■ ASSOCIATED CONTENT

Supporting Information

The Supporting Information is available free of charge at https://pubs.acs.org/doi/10.1021/acsami.1c06243.

Illustration of the traditional NATM fabrication method, estimation of defect density using the obtained Raman data, estimation of defect density using AC-STEM images, simulation of oxygen plasma, SEM images of transferred graphene on the PCTE, discussion of nanopore merging, and discussion of defect size-influenced $I(D)/I(G)$ (PDF)

■ AUTHOR INFORMATION

Corresponding Author

Luda Wang − *Institute of Microelectronics, School of Electronics Engineering and Computer Science, Academy for Advanced Interdisciplinary Studies, and Center for Nanochemistry, Beijing Science and Engineering Center for Nanocarbons, College of Chemistry and Molecular Engineering, Peking University, Beijing 100871, China; Beijing Graphene Institute, Beijing 100095, China;* orcid.org/0000-0001-6222-7807; Email: luda.wang@pku.edu.cn

Authors

Xiaobo Chen − *Institute of Microelectronics, School of Electronics Engineering and Computer Science, Peking University, Beijing 100871, China*

Shengping Zhang − *Institute of Microelectronics, School of Electronics Engineering and Computer Science, Academy for Advanced Interdisciplinary Studies, and Center for Nanochemistry, Beijing Science and Engineering Center for Nanocarbons, College of Chemistry and Molecular Engineering, Peking University, Beijing 100871, China; Beijing Graphene Institute, Beijing 100095, China*

Dandan Hou − *Institute of Microelectronics, School of Electronics Engineering and Computer Science, Peking University, Beijing 100871, China; Beijing Graphene Institute, Beijing 100095, China*

Hongwei Duan − *Institute of Microelectronics, School of Electronics Engineering and Computer Science and Academy for Advanced Interdisciplinary Studies, Peking University, Beijing 100871, China*

Bing Deng − *Center for Nanochemistry, Beijing Science and Engineering Center for Nanocarbons, Beijing National Laboratory for Molecular Sciences, College of Chemistry and Molecular Engineering, Peking University, Beijing 100871, China;* orcid.org/0000-0003-0530-8410

Zhiyang Zeng − *Institute of Microelectronics, School of Electronics Engineering and Computer Science, Peking University, Beijing 100871, China*

Bingyao Liu − *Academy for Advanced Interdisciplinary Studies, Center for Nanochemistry, Beijing Science and*

Engineering Center for Nanocarbons, College of Chemistry and Molecular Engineering, and Electron Microscopy Laboratory, School of Physics, Peking University, Beijing 100871, China; Beijing Graphene Institute, Beijing 100095, China

Luzhao Sun − *Center for Nanochemistry, Beijing Science and Engineering Center for Nanocarbons, Beijing National Laboratory for Molecular Sciences, College of Chemistry and Molecular Engineering, Peking University, Beijing 100871, China*

Ruiyang Song − *Institute of Microelectronics, School of Electronics Engineering and Computer Science, Peking University, Beijing 100871, China*

Jinlong Du − *Electron Microscopy Laboratory, School of Physics, Peking University, Beijing 100871, China*

Peng Gao − *Academy for Advanced Interdisciplinary Studies, Electron Microscopy Laboratory, School of Physics, and International Center for Quantum Materials, School of Physics, Peking University, Beijing 100871, China; Beijing Graphene Institute, Beijing 100095, China; Collaborative Innovation Center of Quantum Matter, Beijing 100871, China;* orcid.org/0000-0003-0860-5525

Hailin Peng − *Center for Nanochemistry, Beijing Science and Engineering Center for Nanocarbons, Beijing National Laboratory for Molecular Sciences, College of Chemistry and Molecular Engineering, Peking University, Beijing 100871, China; Beijing Graphene Institute, Beijing 100095, China;* orcid.org/0000-0003-1569-0238

Zhongfan Liu − *Center for Nanochemistry, Beijing Science and Engineering Center for Nanocarbons, Beijing National Laboratory for Molecular Sciences, College of Chemistry and Molecular Engineering, Peking University, Beijing 100871, China; Beijing Graphene Institute, Beijing 100095, China;* orcid.org/0000-0003-0065-7988

Complete contact information is available at: https://pubs.acs.org/10.1021/acsami.1c06243

Notes

The authors declare no competing financial interest.

■ ACKNOWLEDGMENTS

The authors acknowledge funding from the National Natural Science Foundation of China (NSFC no.62004004) and the Peking University "Health Science-Information Science" Cross-Research Seed Foundation. X.C. also acknowledges financial support from the Boya postdoctoral fellowship. S.Z., D.H., and L.W. acknowledge research fund provided by the Beijing Municipal Science & Technology Commission (no. Z191100000819008), China. We thank the Electron Microscopy Laboratory of Peking University for the use of their electron microscope.

■ REFERENCES

(1) Bakajin, O.; Noy, A. Proteins Make for Finer Filters. *Nat. Nanotechnol.* **2009**, *4*, 345−346.

(2) Wang, L.; Boutilier, M. S. H.; Kidambi, P. R.; Jang, D.; Hadjiconstantinou, N. G.; Karnik, R. Fundamental Transport Mechanisms, Fabrication and Potential Applications of Nanoporous Atomically Thin Membranes. *Nat. Nanotechnol.* **2017**, *12*, 509.

(3) Yang, F.; Tao, F.; Li, C.; Gao, L.; Yang, P. Self-Assembled Membrane Composed of Amyloid-Like Proteins for Efficient Size-Selective Molecular Separation and Dialysis. *Nat. Commun.* **2018**, *9*, 5443.

(4) Baker, R. W. *Membrane Technology and Applications*; Wiley: Newark, California, 2012.

(5) Wijmans, J. G.; Baker, R. W. The Solution-Diffusion Model: A Review. *J. Membr. Sci.* **1995**, *107*, 1−21.

(6) Park, H. B.; Jung, C. H.; Lee, Y. M.; Hill, A. J.; Pas, S. J.; Mudie, S. T.; Van Wagner, E.; Freeman, B. D.; Cookson, D. J. Polymers with Cavities Tuned for Fast Selective Transport of Small Molecules and Ions. *Science* **2007**, *318*, 254−258.

(7) Park, H. B.; Kamcev, J.; Robeson, L. M.; Elimelech, M.; Freeman, B. D. Maximizing the Right Stuff: The Trade-Off between Membrane Permeability and Selectivity. *Science* **2017**, *356*, eaab0530.

(8) Gin, D. L.; Noble, R. D. Designing the Next Generation of Chemical Separation Membranes. *Science* **2011**, *332*, 674−676.

(9) Robeson, L. M. The Upper Bound Revisited. *J. Membr. Sci.* **2008**, *320*, 390−400.

(10) Werber, J. R.; Osuji, C. O.; Elimelech, M. Materials for Next-Generation Desalination and Water Purification Membranes. *Nat. Rev. Mater.* **2016**, *1*, 16018.

(11) Sun, P.; Wang, K.; Zhu, H. Recent Developments in Graphene-Based Membranes: Structure, Mass-Transport Mechanism and Potential Applications. *Adv. Mater.* **2016**, *28*, 2287−2310.

(12) Liu, G.; Jin, W.; Xu, N. Graphene-Based Membranes. *Chem. Soc. Rev.* **2015**, *44*, 5016−5030.

(13) Drahushuk, L. W.; Wang, L.; Koenig, S. P.; Bunch, J. S.; Strano, M. S. Analysis of Time-Varying, Stochastic Gas Transport through Graphene Membranes. *ACS Nano* **2016**, *10*, 786−795.

(14) Berry, V. Impermeability of Graphene and Its Applications. *Carbon* **2013**, *62*, 1−10.

(15) Deng, B.; Liu, Z.; Peng, H. Toward Mass Production of Cvd Graphene Films. *Adv. Mater.* **2019**, *31*, 1800996.

(16) Koenig, S. P.; Wang, L.; Pellegrino, J.; Bunch, J. S. Selective Molecular Sieving through Porous Graphene. *Nat. Nanotechnol.* **2012**, *7*, 728.

(17) Wang, L.; Drahushuk, L. W.; Cantley, L.; Koenig, S. P.; Liu, X.; Pellegrino, J.; Strano, M. S.; Scott Bunch, J. Molecular Valves for Controlling Gas Phase Transport Made from Discrete ångström-Sized Pores in Graphene. *Nat. Nanotechnol.* **2015**, *10*, 785.

(18) Jain, T.; Rasera, B. C.; Guerrero, R. J. S.; Boutilier, M. S. H.; O'Hern, S. C.; Idrobo, J.-C.; Karnik, R. Heterogeneous Sub-Continuum Ionic Transport in Statistically Isolated Graphene Nanopores. *Nat. Nanotechnol.* **2015**, *10*, 1053.

(19) Yuan, Z.; Govind Rajan, A.; Misra, R. P.; Drahushuk, L. W.; Agrawal, K. V.; Strano, M. S.; Blankschtein, D. Mechanism and Prediction of Gas Permeation through Sub-Nanometer Graphene Pores: Comparison of Theory and Simulation. *ACS Nano* **2017**, *11*, 7974−7987.

(20) Huang, S.; Dakhchoune, M.; Luo, W.; Oveisi, E.; He, G.; Rezaei, M.; Zhao, J.; Alexander, D. T. L.; Züttel, A.; Strano, M. S.; Agrawal, K. V. Single-Layer Graphene Membranes by Crack-Free Transfer for Gas Mixture Separation. *Nat. Commun.* **2018**, *9*, 2632.

(21) Denis, P. A.; Iribarne, F. Comparative Study of Defect Reactivity in Graphene. *J. Phys. Chem. C* **2013**, *117*, 19048−19055.

(22) Srinivasu, K.; Ghosh, S. K. Graphyne and Graphdiyne: Promising Materials for Nanoelectronics and Energy Storage Applications. *J. Phys. Chem. C* **2012**, *116*, 5951−5956.

(23) Kidambi, P. R.; Nguyen, G. D.; Zhang, S.; Chen, Q.; Kong, J.; Warner, J.; Li, A.-P.; Karnik, R. Facile Fabrication of Large-Area Atomically Thin Membranes by Direct Synthesis of Graphene with Nanoscale Porosity. *Adv. Mater.* **2018**, *30*, 1804977.

(24) Chen, T.; Li, W.-Q.; Chen, X.-J.; Guo, Y.-Z.; Hu, W.-B.; Hu, W.-J.; Liu, Y. A.; Yang, H.; Wen, K. A Triazine-Based Analogue of Graphyne: Scalable Synthesis and Applications in Photocatalytic Dye Degradation and Bacterial Inactivation. *Chem. − Eur. J.* **2020**, *26*, 2269−2275.

(25) Wu, B.; Li, M.; Xiao, S.; Qu, Y.; Qiu, X.; Liu, T.; Tian, F.; Li, H.; Xiao, S. A Graphyne-Like Porous Carbon-Rich Network Synthesized Via Alkyne Metathesis. *Nanoscale* **2017**, *9*, 11939−11943.

(26) Surwade, S. P.; Smirnov, S. N.; Vlassiouk, I. V.; Unocic, R. R.; Veith, G. M.; Dai, S.; Mahurin, S. M. Water Desalination Using Nanoporous Single-Layer Graphene. *Nat. Nanotechnol.* **2015**, *10*, 459.
(27) Yang, Y.; Yang, X.; Liang, L.; Gao, Y.; Cheng, H.; Li, X.; Zou, M.; Ma, R.; Yuan, Q.; Duan, X. Large-Area Graphene-Nanomesh/Carbon-Nanotube Hybrid Membranes for Ionic and Molecular Nanofiltration. *Science* **2019**, *364*, 1057−1062.
(28) Choi, K.; Droudian, A.; Wyss, R. M.; Schlichting, K.-P.; Park, H. G. Multifunctional Wafer-Scale Graphene Membranes for Fast Ultrafiltration and High Permeation Gas Separation. *Sci. Adv.* **2018**, *4*, No. eaau0476.
(29) O'Hern, S. C.; Boutilier, M. S. H.; Idrobo, J.-C.; Song, Y.; Kong, J.; Laoui, T.; Atieh, M.; Karnik, R. Selective Ionic Transport through Tunable Subnanometer Pores in Single-Layer Graphene Membranes. *Nano Lett.* **2014**, *14*, 1234−1241.
(30) Jang, D.; Idrobo, J.-C.; Laoui, T.; Karnik, R. Water and Solute Transport Governed by Tunable Pore Size Distributions in Nanoporous Graphene Membranes. *ACS Nano* **2017**, *11*, 10042−10052.
(31) Schlichting, K.-P.; Poulikakos, D. Selective Etching of Graphene Membrane Nanopores: From Molecular Sieving to Extreme Permeance. *ACS Appl. Mater. Interfaces* **2020**, *12*, 36468−36477.
(32) Zhao, J.; He, G.; Huang, S.; Villalobos, L. F.; Dakhchoune, M.; Bassas, H.; Agrawal, K. V. Etching Gas-Sieving Nanopores in Single-Layer Graphene with an Angstrom Precision for High-Performance Gas Mixture Separation. *Sci. Adv.* **2019**, *5*, No. eaav1851.
(33) Koizumi, K.; Boero, M.; Shigeta, Y.; Oshiyama, A. Atom-Scale Reaction Pathways and Free-Energy Landscapes in Oxygen Plasma Etching of Graphene. *J. Phys. Chem. Lett.* **2013**, *4*, 1592−1596.
(34) Ferrari, A. C.; Meyer, J. C.; Scardaci, V.; Casiraghi, C.; Lazzeri, M.; Mauri, F.; Piscanec, S.; Jiang, D.; Novoselov, K. S.; Roth, S.; Geim, A. K. Raman Spectrum of Graphene and Graphene Layers. *Phys. Rev. Lett.* **2006**, *97*, 187401.
(35) Ferrari, A. C.; Basko, D. M. Raman Spectroscopy as a Versatile Tool for Studying the Properties of Graphene. *Nat. Nanotechnol.* **2013**, *8*, 235−246.
(36) Eckmann, A.; Felten, A.; Verzhbitskiy, I.; Davey, R.; Casiraghi, C. Raman Study on Defective Graphene: Effect of the Excitation Energy, Type, and Amount of Defects. *Phys. Rev. B* **2013**, *88*, No. 035426.
(37) Xu, X.; Zhang, Z.; Dong, J.; Yi, D.; Niu, J.; Wu, M.; Lin, L.; Yin, R.; Li, M.; Zhou, J.; Wang, S.; Sun, J.; Duan, X.; Gao, P.; Jiang, Y.; Wu, X.; Peng, H.; Ruoff, R. S.; Liu, Z.; Yu, D.; et al. Ultrafast Epitaxial Growth of Metre-Sized Single-Crystal Graphene on Industrial Cu Foil. *Sci. Bull.* **2017**, *62*, 1074−1080.
(38) Yan, Z.; Lin, J.; Peng, Z.; Sun, Z.; Zhu, Y.; Li, L.; Xiang, C.; Samuel, E. L.; Kittrell, C.; Tour, J. M. Toward the Synthesis of Wafer-Scale Single-Crystal Graphene on Copper Foils. *ACS Nano* **2012**, *6*, 9110−9117.
(39) Hao, Y.; Wang, Y.; Wang, L.; Ni, Z.; Wang, Z.; Wang, R.; Koo, C.; Shen, Z.; Thong, J. T. Probing Layer Number and Stacking Order of Few-Layer Graphene by Raman Spectroscopy. *Small* **2010**, *6*, 195−200.
(40) Yoon, D.; Moon, H.; Cheong, H.; Choi, J. S.; Choi, J. A.; Park, B. H. Variations in the Raman Spectrum as a Function of the Number of Graphene Layers. *J. Korean Phys. Soc.* **2009**, *55*, 1299−1303.
(41) Wu, J. B.; Lin, M. L.; Cong, X.; Liu, H. N.; Tan, P. H. Raman Spectroscopy of Graphene-Based Materials and Its Applications in Related Devices. *Chem. Soc. Rev.* **2018**, *47*, 1822−1873.
(42) Fan, L.; Wang, K.; Wei, J.; Zhong, M.; Wu, D.; Zhu, H. Correlation between Nanoparticle Location and Graphene Nucleation in Chemical Vapour Deposition of Graphene. *J. Mater. Chem. A* **2014**, *2*, 13123−13128.
(43) López-Polín, G.; Gómez-Navarro, C.; Parente, V.; Guinea, F.; Katsnelson, M. I.; Pérez-Murano, F.; Gómez-Herrero, J. Increasing the Elastic Modulus of Graphene by Controlled Defect Creation. *Nat. Phys.* **2014**, *11*, 26.
(44) Ugeda, M. M.; Brihuega, I.; Guinea, F.; Gomez-Rodriguez, J. M. Missing Atom as a Source of Carbon Magnetism. *Phys. Rev. Lett.* **2010**, *104*, No. 096804.
(45) Vinchon, P.; Glad, X.; Robert Bigras, G.; Martel, R.; Stafford, L. Preferential Self-Healing at Grain Boundaries in Plasma-Treated Graphene. *Nat. Mater.* **2020**, 49−54.
(46) Gokus, T.; Nair, R. R.; Bonetti, A.; Böhmler, M.; Lombardo, A.; Novoselov, K. S.; Geim, A. K.; Ferrari, A. C.; Hartschuh, A. Making Graphene Luminescent by Oxygen Plasma Treatment. *ACS Nano* **2009**, *3*, 3963−3968.
(47) Beams, R.; Cancado, L. G.; Novotny, L. Raman Characterization of Defects and Dopants in Graphene. *J. Phys.: Condens. Matter* **2015**, *27*, 083002.
(48) Eckmann, A.; Felten, A.; Mishchenko, A.; Britnell, L.; Krupke, R.; Novoselov, K. S.; Casiraghi, C. Probing the Nature of Defects in Graphene by Raman Spectroscopy. *Nano Lett.* **2012**, *12*, 3925−3930.
(49) Jiang, J.; Pachter, R.; Mehmood, F.; Islam, A. E.; Maruyama, B.; Boeckl, J. J. A Raman Spectroscopy Signature for Characterizing Defective Single-Layer Graphene: Defect-Induced I(D)/I(D′) Intensity Ratio by Theoretical Analysis. *Carbon* **2015**, *90*, 53−62.
(50) O'Hern, S. C.; Jang, D.; Bose, S.; Idrobo, J.-C.; Song, Y.; Laoui, T.; Kong, J.; Karnik, R. Nanofiltration across Defect-Sealed Nanoporous Monolayer Graphene. *Nano Lett.* **2015**, *15*, 3254−3260.
(51) Cançado, L. G.; Jorio, A.; Ferreira, E. H. M.; Stavale, F.; Achete, C. A.; Capaz, R. B.; Moutinho, M. V. O.; Lombardo, A.; Kulmala, T. S.; Ferrari, A. C. Quantifying Defects in Graphene Via Raman Spectroscopy at Different Excitation Energies. *Nano Lett.* **2011**, *11*, 3190−3196.
(52) Lucchese, M. M.; Stavale, F.; Ferreira, E. H. M.; Vilani, C.; Moutinho, M. V. O.; Capaz, R. B.; Achete, C. A.; Jorio, A. Quantifying Ion-Induced Defects and Raman Relaxation Length in Graphene. *Carbon* **2010**, *48*, 1592−1597.
(53) O'Hern, S. C.; Stewart, C. A.; Boutilier, M. S. H.; Idrobo, J.-C.; Bhaviripudi, S.; Das, S. K.; Kong, J.; Laoui, T.; Atieh, M.; Karnik, R. Selective Molecular Transport through Intrinsic Defects in a Single Layer of Cvd Graphene. *ACS Nano* **2012**, *6*, 10130−10138.
(54) Qi, Y.; Deng, B.; Guo, X.; Chen, S.; Gao, J.; Li, T.; Dou, Z.; Ci, H.; Sun, J.; Chen, Z.; Wang, R.; Cui, L.; Chen, X.; Chen, K.; Wang, H.; Wang, S.; Gao, P.; Rummeli, M. H.; Peng, H.; Zhang, Y.; et al. Switching Vertical to Horizontal Graphene Growth Using Faraday Cage-Assisted Pecvd Approach for High-Performance Transparent Heating Device. *Adv. Mater.* **2018**, *30*, 1704839.
(55) Pollard, A. J.; Brennan, B.; Stec, H.; Tyler, B. J.; Seah, M. P.; Gilmore, I. S.; Roy, D. Quantitative Characterization of Defect Size in Graphene Using Raman Spectroscopy. *Appl. Phys. Lett.* **2014**, *105*, 253107.
(56) Maguire, P.; Fox, D. S.; Zhou, Y.; Wang, Q.; O'Brien, M.; Jadwiszczak, J.; Cullen, C. P.; McManus, J.; Bateman, S.; McEvoy, N.; Duesberg, G. S.; Zhang, H. Defect Sizing, Separation, and Substrate Effects in Ion-Irradiated Monolayer Two-Dimensional Materials. *Phys. Rev. B* **2018**, *98*, 134109.
(57) Latawiec, P.; Burek, M. J.; Sohn, Y.-I.; Lončar, M. Faraday Cage Angled-Etching of Nanostructures in Bulk Dielectrics. *J. Vac. Sci. Technol., B* **2016**, *34*, No. 041801.
(58) Qiu, X.; Yu, H.; Karunakaran, M.; Pradeep, N.; Nunes, S. P.; Peinemann, K.-V. Selective Separation of Similarly Sized Proteins with Tunable Nanoporous Block Copolymer Membranes. *ACS Nano* **2013**, *7*, 768−776.
(59) Shevate, R.; Kumar, M.; Karunakaran, M.; Canlas, C.; Peinemann, K. V. Surprising Transformation of a Block Copolymer into a High Performance Polystyrene Ultrafiltration Membrane with a Hierarchically Organized Pore Structure. *J. Mater. Chem. A* **2018**, *6*, 4337−4345.
(60) Zhu, G.-d.; Ying, Y.-r.; Li, X.; Liu, Y.; Yang, C.-y.; Yi, Z.; Gao, C.-j. Isoporous Membranes with Sub-10 Nm Pores Prepared from Supramolecular Interaction Facilitated Block Copolymer Assembly and Application for Protein Separation. *J. Membr. Sci.* **2018**, *566*, 25−34.

https://doi.org/10.1021/acsami.1c06243
ACS Appl. Mater. Interfaces 2021, 13, 29926−29935

(61) Luo, X.; Tang, C. Y.; Zhu, X.; Xu, D.; Xing, J.; Lin, D.; Liu, Y.; Yang, L.; Song, J.; Gan, Z.; Li, G.; Liang, H. Tunable Isoporous Ceramic Membranes Towards Precise Sieving of Nanoparticles and Proteins. *J. Membr. Sci.* **2021**, *634*, 119391.
(62) Fan, J.-P.; Zhang, F.-Y.; Yang, X.-M.; Zhang, X.-H.; Cao, Y.-H.; Peng, H.-L. Preparation of a Novel Supermacroporous Molecularly Imprinted Cryogel Membrane with a Specific Ionic Liquid for Protein Recognition and Permselectivity. *J. Appl. Polym. Sci.* **2018**, *135*, 46740.
(63) Ignacio-de Leon, P. A. A.; Eygeris, Y.; Haynes, R.; Zharov, I. Diffusion of Proteins across Silica Colloidal Crystals. *Langmuir* **2018**, *34*, 10333−10339.
(64) Nguyen, Q. H.; Ali, M.; Bayer, V.; Neumann, R.; Ensinger, W. Charge-Selective Transport of Organic and Protein Analytes through Synthetic Nanochannels. *Nanotechnology* **2010**, *21*, 365701.
(65) Yu, S.; Lee, S. B.; Kang, M.; Martin, C. R. Size-Based Protein Separations in Poly(Ethylene Glycol)-Derivatized Gold Nanotubule Membranes. *Nano Lett.* **2001**, *1*, 495−498.
(66) Humes, H. D.; Buffington, D.; Westover, A. J.; Roy, S.; Fissell, W. H. The Bioartificial Kidney: Current Status and Future Promise. *Pediatr. Nephrol.* **2014**, *29*, 343−351.
(67) Lamer, V. K.; Dinegar, R. H. Theory, Production and Mechanism of Formation of Monodispersed Hydrosols. *J. Am. Chem. Soc.* **1950**, *72*, 4847−4854.
(68) Peng, Z. A.; Peng, X. Nearly Monodisperse and Shape-Controlled Cdse Nanocrystals Via Alternative Routes: Nucleation and Growth. *J. Am. Chem. Soc.* **2002**, *124*, 3343−3353.
(69) Park, J.; Joo, J.; Kwon, S. G.; Jang, Y.; Hyeon, T. Synthesis of Monodisperse Spherical Nanocrystals. *Angew. Chem., Int. Ed.* **2007**, *46*, 4630−4660.
(70) Ronco, C. The Rise of Expanded Hemodialysis. *Blood Purif.* **2017**, *44*, I−VIII.
(71) Ronco, C.; Clark, W. R. Haemodialysis Membranes. *Nat. Rev. Nephrol.* **2018**, *14*, 394−410.

https://doi.org/10.1021/acsami.1c06243
ACS Appl. Mater. Interfaces 2021, 13, 29926−29935